AD-A056 958 AIR FORCE GEOPHYSICS LAB HANSCOM AFB MASS F/G 4/2
CALCULATION OF THE BUOYANT MOTION OF A TURBULENT PLANAR HEATED --ETC(U)
MAR 78 M M KLEIN
UNCLASSIFIED AFGL-TR-78-0072 NL

| OF |
AD
A056958

END
DATE
FILMED
9 -78
DDC

AD A056958

AD No.
DDC FILE COPY

LEVEL II

AFGL-TR-78-0072
AIR FORCE SURVEYS IN GEOPHYSICS, NO. 385

# Calculation of the Buoyant Motion of a Turbulent Planar Heated Jet in an Opposing Air Stream

MILTON M. KLEIN



23 MARCH 1978

Approved for public release; distribution unlimited.

METEOROLOGY DIVISION PROJECT 2093
AIR FORCE GEOPHYSICS LABORATORY
HANSCOM AFB, MASSACHUSETTS 01731

AIR FORCE SYSTEMS COMMAND, USAF

This report has been reviewed by the ESD Information Office (OI) and is releasable to the National Technical Information Service (NTIS).

This technical report has been reviewed and is approved for publication.

FOR THE COMMANDER

John Howard

Chief Scientist

Qualified requestors may obtain additional copies from the Defense Documentation Center. All others should apply to the National Technical Information Service.

Unclassified

SECURITY CLASSIFICATION OF THIS PAGE (When Data Entered)

**REPORT DOCUMENTATION PAGE**

READ INSTRUCTIONS BEFORE COMPLETING FORM

(14) 1. REPORT NUMBER
AFGL-TR-78-0072, AFGL-AFSG-385

2. GOVT ACCESSION NO.

(9) 3. RECIPIENT'S CATALOG NUMBER
Air Force surveys in geophysics,

(6) 4. TITLE (and Subtitle)
CALCULATION OF THE BUOYANT MOTION OF A TURBULENT PLANAR HEATED JET IN AN OPPOSING AIR STREAM

5. TYPE OF REPORT & PERIOD COVERED
Scientific. Interim.

6. PERFORMING ORG. REPORT NUMBER
AFSG No. 385

7. AUTHOR(s)
(10) Milton M./Klein

8. CONTRACT OR GRANT NUMBER(s)

9. PERFORMING ORGANIZATION NAME AND ADDRESS
Air Force Geophysics Laboratory (LYP)
Hanscom AFB
Massachusetts 01731

10. PROGRAM ELEMENT, PROJECT, TASK AREA & WORK UNIT NUMBERS
(16) 62101F (17) 01
2093[redacted]

11. CONTROLLING OFFICE NAME AND ADDRESS
Air Force Geophysics Laboratory (LYP)
Hanscom AFB
Massachusetts 01731

(11) 12. REPORT DATE
23 Mar[redacted]78

(12) 13. NUMBER OF PAGES
34 P.

14. MONITORING AGENCY NAME & ADDRESS (if different from Controlling Office)

15. SECURITY CLASS. (of this report)
Unclassified

15a. DECLASSIFICATION/DOWNGRADING SCHEDULE

16. DISTRIBUTION STATEMENT (of this Report)

Approved for public release; distribution unlimited.

17. DISTRIBUTION STATEMENT (of the abstract entered in Block 20, if different from Report)

18. SUPPLEMENTARY NOTES

19. KEY WORDS (Continue on reverse side if necessary and identify by block number)

Thermal fog dispersion
Counterflowing jet
Heated jet
Planar jet
Buoyancy
Turbulence

20. ABSTRACT (Continue on reverse side if necessary and identify by block number)

A broad experimental and theoretical program is being conducted to aid in the development of an operational warm fog dispersal system which utilizes momentum driven ground based heat sources. To help determine optimum heat and thrust combinations for the system, investigations are being made of the buoyant motion of heated turbulent jets both coflowing (wind and jet in the same direction) and counterflowing (wind and jet opposite). The investigation of the coflowing jet has been completed and in addition a model has been developed next page

DD FORM 1 JAN 73 1473 EDITION OF 1 NOV 65 IS OBSOLETE

Unclassified

SECURITY CLASSIFICATION OF THIS PAGE (When Data Entered)

449 578

78 07 31 154

hc

20. Abstract (Continued)

from which the dynamic characteristics of a heated counterflowing jet in the absence of buoyancy can be calculated. The present investigation is concerned with the effect of buoyancy upon the motion of a counterflowing jet.

The lower portion of the trajectory, which has been calculated by the present model, is in fair to good agreement with the corresponding experimental curve, the calculated curve tending to be somewhat higher than that obtained experimentally. The calculated upper part of the trajectory, obtained from a model which gives the deflection of a jet in a crosswind, is in good agreement with experiment.

The present model yields a scaling law for a counterflowing jet which indicates that the scaling depends principally upon the Froude number defined by the initial jet velocity and excess temperature and very weakly upon the initial jet temperature. This result is essentially the same as that obtained for the coflowing jet for the case of small values of windspeed relative to initial jet velocity.

# Preface

The author would like to thank Mr. Bruce A. Kunkel for his critical review and constructive criticism of the final manuscript.

## Contents

## Illustrations

# Calculation of the Buoyant Motion of a Turbulent Planar Heated Jet in an Opposing Air Stream

## 1. INTRODUCTION

As part of the development of an operational Warm Fog Dispersal System (WFDS), experimental and theoretical studies have been made of the characteristics of ground based heated jets for various combinations of heat and thrust under different wind conditions. The dynamic characteristics of a nonbuoyant coflowing jet, that is, jet in the same direction as the wind, are well known and presented in detail by Abramovich.[1] The method of calculating the buoyant motion of a heated submerged jet, that is, no wind, (Abramovich[2]) can be extended in a straightforward manner to the case of the coflowing jet, planar or round (Klein and Kunkel[3, 4]). For simplicity, the attachment of the jet to the ground (ground effect) was neglected in

(Received for publication 22 March 1978)

1. Abramovich, G. N. (1963) The Theory of Turbulent Jets, The MIT Press, Cambridge, Mass., Chapters 4 and 5.
2. Abramovich, G. N. (1963) The Theory of Turbulent Jets, The MIT Press, Cambridge, Mass., Chapter 12, pp 580-585.
3. Klein, M. M., and Kunkel, B. A. (1975) Interaction of a Buoyant Turbulent Planar Jet With a Coflowing Wind, AFCRL-TR-75-0368.
4. Klein, M. M., and Kunkel, B. A. (1975) Interaction of a Buoyant Turbulent Round Jet With a Coflowing Wind, AFCRL-TR-75-0581.

these investigations. A method of taking into account the ground effect for a coflowing jet has been developed by Klein.[5]

The situation for the nonbuoyant counterflowing jet, that is, jet and wind directions opposite, as presented by Abramovich,[6] is considerably less satisfactory both with regard to theory and experiment. Here the calculations, which must account for the regions of counterflow, are quite specialized and not easily adapted to the buoyant jet. Recently, however, a simplified model for a counterflowing round jet has been developed by Sekundov,[7] which may be extended in a straightforward manner to take account of buoyancy and obtain the jet trajectories. An important feature of the Sekundov model is the use of a finite wall to help simplify the equations of motion. The results for an open jet are then obtained by making the wall arbitrarily large. The Sekundov model, which is limited to the case of an unheated incompressible jet, has been extended to take account of heat addition and density variation, while neglecting the buoyant motion (Klein[8]). The present investigation is concerned with the buoyant motion of the counterflowing jet. Since the jets in the warm fog dispersal system merge a short distance downstream of the jet nozzles,[9] the investigation, parallel to that reference 8, has been confined to the planar case.

As in the case of the coflowing jet, experiments[9] show that the counterflowing jet also remains attached to the ground for some distance downstream of the nozzle, resulting in a delayed lift-off point. A method of analysis similar to that of reference 5 was utilized to determine the point of lift-off.

## 2. JET GEOMETRY

A schematic sketch of the flow pattern for a planar jet is shown in Figure 1a while the corresponding trajectory of the jet centerline is given in Figure 1b. Here u and T denote velocity and temperature, while the subscripts o, m and a designate initial, axial and ambient values. In the initial section, where the

5. Klein, M.M. (1977) A Method for Determining the Point of Lift-Off and Modified Trajectory of a Ground-Based Heated Turbulent Planar Jet in a Coflowing Wind, AFGL-TR-77-0033.
6. Abramovich, G.N. (1963) The Theory of Turbulent Jets, The MIT Press, Cambridge, Mass., Chapters 4 and 9.
7. Sekundov, A.N. (1969) The Propagation of a Turbulent Jet in an Opposing Stream, in Turbulent Jets of Air, Plasma and Real Gas, Consultants Bureau, New York.
8. Klein, M.M. (1977) Interaction of a Turbulent Planar Heated Jet With a Counterflowing Wind, AFGL-TR-77-0214.
9. Kunkel, B.A. (1975) Heat and Thrust Requirements of a Thermal Fog Dispersal System, AFCRL-TR-75-0472.

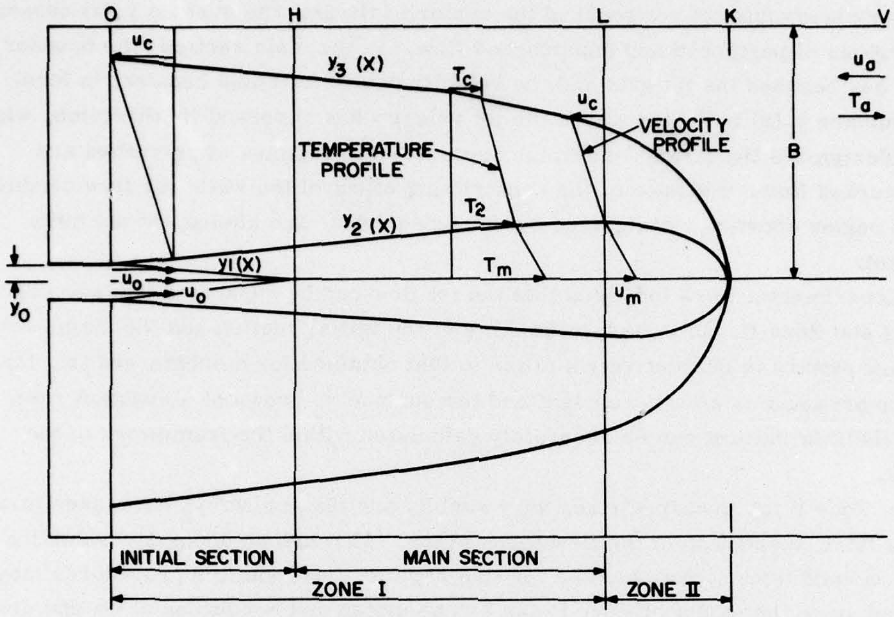


Figure 1a. Schematic Representation of Geometry of Counterflowing Jet and Velocity and Temperature Profiles

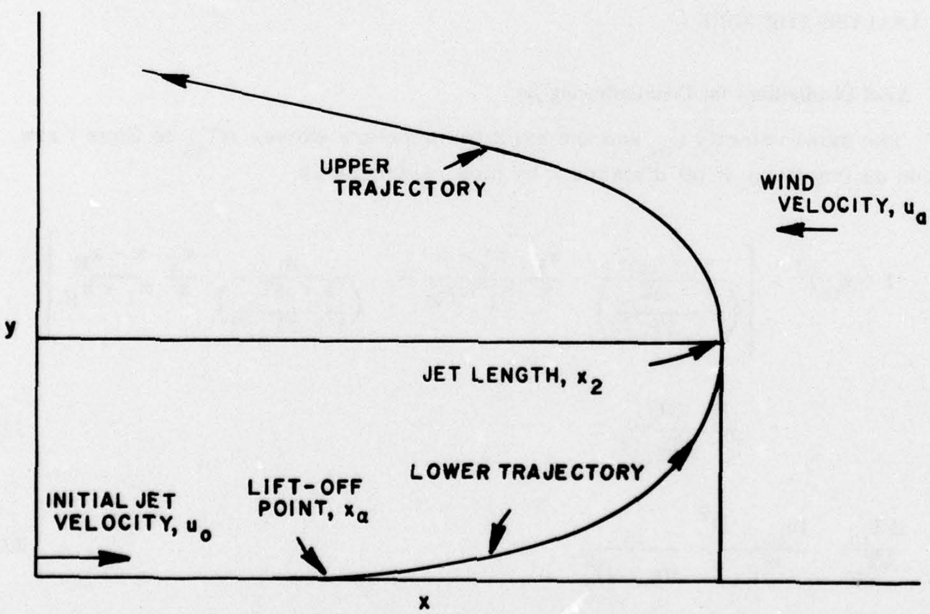


Figure 1b. Schematic Representation of Jet Centerline Trajectory

boundary layer has not yet reached the center of the jet, the surface $y_1(x)$ separates the regions of perturbed and unperturbed flow. In the main section the boundary layer has reached the jet axis and the velocity profile remains constant in form. The surface $y_2(x)$ indicates where the jet velocity has reversed its direction, while $y_3(x)$ designates the streamline which separates the regimes of perturbed and unperturbed flow. Because of the constricting effect of the walls the flow conditions in the region above $y_3$, designated by the subscript c, are almost but not quite ambient.

Experimental work indicates that the jet flow can be separated into two regimes, Zone I and Zone II. In Zone I, consisting of the initial section and the main section, the flow pattern is qualitatively similar to that obtained for a submerged jet, that is, the pressure is almost constant and the surface $y_2$ grows at a constant rate. Here the flow pattern can be accurately calculated within the framework of the model.

In Zone II the pressure rises very rapidly and the surface $y_2$ decreases to zero as the final retardation of the flow takes place. Although an accurate evaluation of the flow conditions is not possible for this regime, interpolative procedures may be used since the extent of Zone II can be calculated and conditions at its end are known.

## 3. ANALYSIS FOR ZONE I

### 3.1 Axial Distributions for Counterflowing Jet

The axial velocity $u_m$ and the axial temperature excess $\Delta T_m$ in Zone I are given as functions of jet distance x by (see reference 8)

$$(1 + u_m)^2 = \left[ \frac{(1+m)^2}{\left(\frac{1+\Delta T_o}{1+\Delta T_o/2}\right)} \frac{x_H}{x} \frac{x_1 - x}{x_1 - x_H} + \frac{4}{\left(\frac{1+\Delta T_1}{1+\Delta T_1/2}\right)} \frac{x_1}{x} \frac{x - x_H}{x_1 - x_H} \right]$$

$$\frac{1+\Delta T_m}{1+\Delta T_m/2} \tag{1}$$

$$\frac{\Delta T_m}{\Delta T_o} = \frac{(u_m+1)^2}{u_m} \frac{m}{(m+1)^2} \tag{2}$$

where $\Delta T_m$ is the temperature excess over ambient, m is the dimensionless value of the initial jet velocity $u_o$ referred to ambient, and the subscripts H and 1 refer to the ends of the initial and main sections. As in reference 8, velocity, density, temperature and length are taken as dimensionless, referring to initial jet half width $y_o$ for length and to ambient values for the other quantities.

The analysis presented in reference 8 shows that the temperature variation given by Eq. (2) is somewhat slower in the outer region of the jet than that given by experiment. We shall, therefore, utilize in place of Eq. (2) the linear form

$$\frac{\Delta T_m}{\Delta T_o} = \frac{1 + u_m}{1 + m} \tag{3}$$

which is close to Eq. (2) in the initial region of the jet but gives a slightly greater decrease in $\Delta T_m$ in the outer region.

The surface of zero velocity, $y_2(x)$, and the outer boundary of the jet, $y_3(x)$, are obtained from

$$y_2 = cx \tag{4}$$

$$N - 1 = \frac{a_1}{a_o} \rho_m u_m (2u_m + 3) \tag{5}$$

$$a_1 = \frac{1}{2} \left(1 + \frac{\rho_2}{\rho_m}\right) = \frac{1}{2} \left(1 + \frac{1 + \Delta T_m}{1 + \Delta T_2}\right) \tag{6}$$

$$a_o = \frac{1}{2}(1 + \rho_2) = \frac{1}{2} \left(1 + \frac{1}{1 + \Delta T_2}\right) \tag{7}$$

$$\Delta T_2 = \frac{\Delta T_m}{1 + u_m} \tag{8}$$

where $N = \frac{y_3}{y_2}$, c is a growth or mixing coefficient having the value 0.22 for the main region, $\rho$ is density, and the subscript 2 indicates values at the surface $y_2$. Because of the delayed lift-off point and the initial rapid decrease in temperature, the quantities $\Delta T_m$ and $\Delta T_2$ are small compared to unity. It will, therefore, be convenient to develop $a_1$, $a_o$ and $\rho_m$ to 2nd order in $\Delta T_m$ to yield

$$a_1 = 1 + \frac{v - 1}{2v} \Delta T_m - \frac{(v - 1)}{2v^2} \Delta T_m^2 \tag{9}$$

$$a_o = 1 + \frac{1}{2v}\,\Delta T_m - \frac{1}{2v^2}\,\Delta T_m^2 \tag{10}$$

$$\rho_m = 1 - \Delta T_m + \Delta T_m^2 \tag{11}$$

$$N - 1 = (2v + 1)(v - 1)\left[1 - \frac{\Delta T_m}{2} + \frac{\left(v - \frac{1}{2}\right)}{2v}\,\Delta T_m^2\right] \tag{12}$$

where $v = 1 + u_m$.

### 3.2 Calculation of the Buoyant Force

The buoyant force per unit length, B, is obtained from

$$B = 2\,g\rho_a\,y_o^2\left[\int_o^{y_2} (1 - \rho)\,dy + \int_{y_2}^{y_3} (1 - \rho)\,dy\right] \tag{13}$$

where y is the vertical coordinate. In view of the small variation of pressure in the main region we may write

$$\rho = \frac{1}{T} = \frac{1}{1 + \Delta T} \tag{14}$$

and express Eq. (13) as

$$B = 2\,g\rho_a\,y_o^2\left[\int_o^{y_2} \frac{\Delta T}{1 + \Delta T}\,dy + \int_{y_2}^{y_3} \frac{\Delta T}{1 + \Delta T}\,dy\right] \quad . \tag{15}$$

Since $\Delta T$ is small compared to unity at and beyond the lift-off point, we may develop the integrand in Eq. (15) as a power series in $\Delta T$ to yield

$$B = 2\,g\rho_a\,y_o^2\,(I_1 + I_2) \tag{16}$$

$$I_1 = \int_o^{y_2} \Delta T(1 - \Delta T + \Delta T^2 - \Delta T^3 + \ldots)\,dy \tag{17}$$

$$I_2 = \int_{y_2}^{y_3} \Delta T(1 - \Delta T + \Delta T^2 - \Delta T^3 + \ldots)\, dy \quad . \tag{18}$$

To evaluate $I_1$ and $I_2$, and for subsequent analysis, we require the velocity and temperature profiles. Utilizing the linear profiles of reference 8, for the region $0 \leqq y \leqq y_2$:

$$\frac{u}{u_m} = 1 - \frac{y}{y_2} \tag{19}$$

$$\frac{\Delta T}{\Delta T_m} = \frac{u + 1}{u_{m+1}} = 1 - \frac{y}{a y_2} \tag{20}$$

$$a = 1 + \frac{1}{u_m}$$

$$\frac{\Delta T_2}{\Delta T_m} = \frac{1}{1 + u_m} \quad . \tag{21}$$

For the region $y_2 \leqq y \leqq y_3$:

$$u = \frac{y - y_2}{y_3 - y_2} \tag{22}$$

$$\frac{\Delta T}{\Delta T_2} = 1 - u = 1 - \frac{y - y_2}{y_3 - y_2} \tag{23}$$

we obtain for $I_1$ and $I_2$,

$$I_1 = y_2\, \Delta T_m \left[1 - \frac{1}{2a} - \Delta T_m \left(1 - \frac{1}{a} + \frac{1}{3a^2}\right) + \Delta T_m^2 \left(1 - \frac{3}{2a} + \frac{1}{a^2} - \frac{1}{4a^3}\right)\right] \tag{24}$$

$$I_2 = y_2(N - 1)\, \frac{\Delta T_2}{2} \left(1 - \frac{2}{3}\, \Delta T_2 + \frac{\Delta T_2^2}{2}\right) \quad . \tag{25}$$

Employing Eqs. (8) and (12) for $\Delta T_2$ and N - 1, and expressing a in terms of v by

$$a = \frac{1}{1 - \frac{1}{v}} \tag{26}$$

allows us to write Eqs. (24) and (25) in the form

$$I_1 = y_2 \, \Delta T_m \left[ \frac{1}{2} \left( 1 + \frac{1}{v} \right) - \frac{\Delta T_m}{3} \left( 1 + \frac{1}{v} + \frac{1}{v^2} \right) + \frac{\Delta T_m^2}{4} \left( 1 + \frac{1}{v} + \frac{1}{v^2} + \frac{1}{v^3} \right) \right] \tag{27}$$

$$I_2 = y_2 \, \Delta T_m \left( v - \frac{1}{2} - \frac{1}{2v} \right) \left[ 1 - \frac{\Delta T_m}{2} \left( 1 + \frac{4}{3v} \right) + \Delta T_m^2 \left( 1 + \frac{1}{12\,v} + \frac{1}{2v^2} \right) \right] \quad . \tag{28}$$

Addition of Eqs. (27) and (28) then yields for the buoyant force in Zone I.

$$B = 2\, g \rho_a \, y_o^2 \, y_2 \left[ v\, \Delta T_m - \left( \frac{v}{2} + \frac{3}{4} - \frac{1}{4\,v} \right) \Delta T_m^2 + \left( \frac{v}{2} + \frac{1}{12} + \frac{11}{24\,v} - \frac{1}{24\,v^2} \right) \Delta T_m^3 \right] \quad . \tag{29}$$

### 3.3 Trajectory Analysis

The vertical velocity is determined from the equation

$$\frac{d}{dx}(\phi V) = B \tag{30}$$

where $\phi$ is the mass flux, through the cross section of the boundary layer and given by

$$\phi = \phi_1 + \phi_2 \tag{31}$$

with $\phi_1$ the mass flux through that portion of the boundary layer below $y_2$ and $\phi_2$ the mass flux through the part above $y_2$. We note that, although $\phi_1$ and $\phi_2$ are in opposite directions, $\phi$ is given by the numerical sum of $\phi_1$ and $\phi_2$. This is due to the fact that the equation for the vertical velocity is unaffected by a change in direction of the flux, that is, the vertical velocity increases positively to the right in either case.

The quantities $\phi_1$ and $\phi_2$ are obtained from

$$\phi_1 = 2\rho_a u_a y_o \int_o^{y_2} \rho u \, dy$$

$$\phi_1 = \rho_a u_a a_1 \rho_m u_m y_2 y_o \tag{32}$$

$$\phi_2 = 2\rho_a u_a y_o \int_{y_2}^{y_3} \rho u \, dy$$

$$\phi_2 = \rho_a u_a a_o (N - 1) y_2 y_o = \rho_a u_a a_1 \rho_m u_m (2u_m + 3) y_2 y_o \tag{33}$$

$$\phi = 2\rho_a u_a a_1 \rho_m u_m (2 + u_m) y_2 y_o \tag{34}$$

in which we have used Eq. (5) for N - 1.

The slope of the center line of the jet is given by

$$\frac{dy}{dx} = \frac{\phi V}{P} \tag{35}$$

where P is the momentum flux through the boundary layer and, analogous to the mass flux $\phi$, given by

$$P = P_1 + P_2 \tag{36}$$

$$P_1 = 2\rho_a u_a^2 y_o \int_o^{y_2} \rho u^2 \, dy$$

$$P_1 = \frac{2}{3} \rho_a u_a^2 a_1 \rho_m u_m^2 y_2 y_o \tag{37}$$

$$P_2 = 2\rho_a y_a^2 y_o \int_{y_2}^{y_3} \rho u^2 \, dy$$

$$P_2 = \frac{2}{3} \rho_a u_a^2 a_o (N - 1) y_2 y_o = \frac{2}{3} \rho_a u_a^2 a_1 \rho_m u_m (2u_m + 3) y_2 y_o \tag{38}$$

$$P = 2\rho_a u_a^2 a_1 \rho_m u_m(u_m + 1) \quad . \tag{39}$$

Since the point of lift-off $x_\alpha$ is well downstream of the nozzle, the axial velocity and temperature have dropped considerably below their initial values and vary slowly beyond $x_\alpha$. An inspection of the results of reference 8 shows that the velocity $u_m$ decreases almost linearly with distance x beyond the lift-off point. Therefore, for purposes of integration, it is convenient to replace the cumbersome equation (1) by the simple linear from

$$u_m = u_\alpha - (u_\alpha - 1)\frac{x - x_\alpha}{x_1 - x_\alpha} \quad . \tag{40}$$

Utilizing Eqs. (3) and (4) for $\Delta T_m$ and $y_2$ we may write the integrated form of the buoyancy equation to order $\Delta T_m^2$ in the form

$$\phi V = \phi_\alpha V_\alpha + 2 g \rho_a y_o^2 c \frac{\Delta T_m}{1 + m}\left[I - I_\alpha - \frac{\Delta T_o}{1 + m}(J - J_\alpha)\right] \tag{41}$$

where

$$I - I_\alpha = \int_{x_\alpha}^{x} x v^2 \, dx \tag{42}$$

$$J - J_\alpha = \int_{x_\alpha}^{x} x \left(\frac{v^2}{2} + \frac{3v}{4} - \frac{1}{4v}\right) dx \quad . \tag{43}$$

Numerical checks show that the J integral contributes very little to the vertical velocity V and will therefore be neglected. The I integral is easily evaluated to yield

$$I - I_\alpha = (x_1 - x_\alpha)^2\left[\frac{\beta^2}{2} t^2 - 2\beta(u_\alpha - 1)\frac{t^3}{3} + (u_\alpha - 1)^2\frac{t^4}{4}\right]\Bigg|_{t_\alpha}^{t} \tag{44}$$

where

$$\beta = u_\alpha + 1 + (u_\alpha - 1)\, t_\alpha \tag{45}$$

$$t = \frac{x}{x_1 - x_\alpha} \quad . \tag{46}$$

Making use of Eq. (34) for $\phi$, we may write the vertical velocity equation in the form

$$\frac{V}{u_o} = \frac{x_\alpha}{x} \frac{(v_\alpha^2 - 1)}{v^2 - 1} \frac{f_\alpha}{f} \frac{V_\alpha}{u_o} + \frac{1}{K} \frac{m}{1 + m} \frac{1}{v^2 - 1} \frac{1}{x} (I - I_\alpha) \tag{47}$$

where

$$K = \frac{u_o^2}{y_o\, g\, \Delta T_o} \tag{48}$$

is the Froude number for the flow, and f is the value of $a_1 \rho_m$ in Eq. (34), and given to first order in $\Delta T_o/(1 + m)$ by (see Eqs. (9) and (11))

$$f = 1 - \frac{1 + v}{2} \frac{\Delta T_o}{1 + m} \quad . \tag{49}$$

If we employ Eq. (41) for the vertical velocity, the integrated form of the trajectory Eq. (35) may be written as

$$y = \phi_\alpha V_\alpha \int_{x_\alpha}^{x} \frac{dx}{P} + 2 g \rho_a y_o^2 c \frac{\Delta T_o}{1 + m} \left( \int_{x_\alpha}^{x} \frac{I\, dx}{P} - I_\alpha \int_{x_\alpha}^{x} \frac{dx}{P} \right) \quad . \tag{50}$$

Using Eq. (39) for P, the integrals in Eq. (50) are easily evaluated to yield

$$y = \frac{x_\alpha (v_\alpha^2 - 1)}{v(v - 1)} (K_o - K_1) + \frac{1}{K} \frac{m^2}{1 + m} (K_2 - K_1) - \frac{1}{K} \frac{m^2}{1 + m} I_\alpha (K_o - K_1) \tag{51}$$

where

$$K_o = \frac{1}{\beta - 1}\int_{t_\alpha}^{t} \frac{dt}{t(v-1)} = \frac{1}{\beta - 1} \ell n \left(\frac{t}{v-1}\right)\Bigg|_{t_\alpha}^{t} \tag{52}$$

$$K_1 = \frac{1}{\beta}\int_{t_\alpha}^{t} \frac{dt}{t\,v} = \frac{1}{\beta} \ell n \left(\frac{t}{v}\right)\Bigg|_{t_\alpha}^{t} \tag{53}$$

$$K_2 = \int_{t_\alpha}^{t} \frac{I\,dt}{t(v-1)}\,dt$$

$$K_2 = \left[\frac{(\beta - 1)}{(v_\alpha - 2)^2} a_2 \ell n \left(\frac{1}{v-1}\right) - \frac{a_2}{v_\alpha - 2} t + \frac{5\beta + 3}{24} t^2 - \frac{(v_\alpha - 2)}{12} t^3\right]\Bigg|_{t_\alpha}^{t} \tag{54}$$

$$K_3 = \int_{t_\alpha}^{t} \frac{I\,dt}{t\,v}$$

$$K_3 = \left[\frac{\beta^3}{12(v_\alpha - 2)^2} \ell n \frac{1}{v} - \frac{\beta^2}{12(v_\alpha - 2)} t + \frac{5\beta}{12} t^2 - \frac{(v_\alpha - 2)}{12} t^3\right]\Bigg|_{t_\alpha}^{t} \tag{55}$$

$$a_2 = \frac{\beta^2}{2} - \frac{(5\beta + 3)(\beta - 1)}{12} \tag{56}$$

and we have neglected the small term in $\Delta T_o/(1 + m)$ contributed by f.

### 3.4 Dependence of Vertical Velocity and Trajectory Upon Parameters

The foregoing results give the general dependence of the vertical velocity and trajectory upon the jet parameters and position. Thus, from Eq. (47) the vertical velocity is proportional to $1/K$ while Eq. (51) indicates the trajectory y is proportional to $m/K$. This explicit dependence upon m is due to the separation of m and x in the velocity Eq. (1). It is not present in the trajectory for a coflowing jet[3] where the dependence of vertical velocity upon windspeed is far more complex.

*An examination of Eqs. (47) and (51) shows that the dependence of* $V/u_o$ and y upon position x is more complex than a simple power law. However, an analysis

of numerical solutions of these equations indicates that, roughly, the vertical velocity increases less rapidly than $x^2$ while the trajectory rises more rapidly than $x^2$. These appears to be reasonable results when compared to the coflowing case where $V/u_o \sim x$, $y \sim x^{5/2}$.

### 3.5 Scaling Law for Counterflowing Jet

The foregoing results may be utilized to derive the scaling law for a counterflowing jet. An examination of Eqs. (1) and (2) show that, for constant m, the velocity and temperature distributions are independent of length scale. The right hand side of the trajectory Eq. (35) will, therefore, depend only on the Froude number K during a change of scale at constant m (note that the velocity dependence $v^2 \sim T_o^{-1}$ in both numerator and denominator leads to a weak dependence upon $T_o$ which may be neglected here). This scaling law is in conformity with that obtained for the coflowing jet[3] where it is shown that the trajectory depends principally upon the Froude number, the effect of initial temperature $T_o$ being negligible.

## 4. ANALYSIS FOR ZONE II

### 4.1 Axial Distributions

As indicated previously, the axial velocity and temperature in Zone II do not have a large variation and may be obtained by interpolation. Since $u_m$ has the value unity at $x_1$ and zero at the end of Zone II we write

$$u_m = 1 - S \tag{57}$$

where

$$S = \frac{x - x_1}{x_2 - x_1} \tag{58}$$

and $x_2$ designates the end of Zone II. The experimental data indicates that Eq. (3) for $\Delta T_m$ is fairly accurate in Zone II and will, therefore, be retained in this region.

The surface $y_2(x)$ decreases to zero with a vertical tangent at $x_2$; accordingly, we shall utilize the simple parabolic form

$$y_2 = y_{21}(1 - S)^{1/2} \tag{59}$$

where $y_{21}$ designates the value of $y_2$ at $x_1$.

The experimental data of Vulis[10] indicate that $y_3$ is roughly constant until $y_2$ and $u_m$ have decreased to zero. A short distance further out ambient conditions have been attained. For simplicity we shall, therefore, assume $y_3$ is constant and take the end of Zone II, $x_2$, as the termination of the jet, that is, the location at which the jet reverses its direction. Accordingly, we may now write

$$y_3 = y_{31} = y_{21} N_1 \tag{60}$$

where $y_{31}$, and $N_1$ are the values of $y_3$ and N at $x_1$. From Eqs. (3) and (12), $N_1$ is given by

$$N_1 - 1 = 5 \left[ 1 - \frac{\Delta T_o}{1 + m} + \frac{3}{2} \frac{\Delta T_o^2}{(1 + m)^2} \right] . \tag{61}$$

### 4.2 Determination of the Buoyant Force

The buoyancy at the position $x_1$ is given by the integrals $I_1$ and $I_2$ in Eqs. (24) and (25), but the values of $y_2$, $y_3$, v and N are now given by the equations of Section 4.1. Accordingly we first write the buoyancy B as

$$B = 2 g \rho_a y_o^2 (B_1 + B_2 + B_3) \tag{62}$$

where

$$B_1 = \frac{1}{2} \frac{\Delta T_o}{1 + m} (y_2 v + y_3) \tag{63}$$

$$B_2 = - \frac{1}{3} \frac{\Delta T_o^2}{(1 + m)^2} [y_2(v^2 + v) + y_3] \tag{64}$$

$$B_3 = \frac{1}{4} \frac{\Delta T_o^3}{(1 + m)^3} [y_2(v^3 + v^2 + v) + y_3)] \tag{65}$$

and then use (59), (60) and (61) to cast $B_1$, $B_2$ and $B_3$ into the more explicit form

$$B_1 = \frac{1}{2} \frac{\Delta T_o}{1 + m} y_{21} [(2 - S)(1 - S)^{1/2} + 6] \tag{66}$$

---

10. Abramovich, G. N. (1963) The Theory of Turbulent Jets, The MIT Press, Cambridge, Mass., Chapter 1, pp 32-36.

$$B_2 = -\frac{1}{3}\frac{\Delta T_o^2}{(1+m)^2}\, y_{21}\left\{[(2-S)^2 + (2-S)](1-S)^{1/2} + \frac{27}{2}\right\} \tag{67}$$

$$B_3 = \frac{1}{4}\frac{\Delta T_o^3}{(1+m)^3}\, y_{21}\left\{[(2-S)^3 + (2-S)^2 + (2-S)](1-S)^{1/2} + \frac{83}{3}\right\} . \tag{68}$$

### 4.3 Calculation of the Trajectory

The flux $\phi$ in Zone II is, from Eqs. (32) and (33) now given by

$$\phi = \mu_1 + \mu_2 + \mu_3 \tag{69}$$

$$\mu_1 = \frac{y_2}{2}(v-2) + \frac{y_3}{2} \tag{70}$$

$$\mu_2 = \frac{-\Delta T_o}{4(1+m)}\,[y_2(v^2-2) + y_3] \tag{71}$$

$$\mu_3 = \frac{\Delta T_o^2}{4(1+m)^2}\,\{y_2[(v-1)(v^2+1) - 1]\} \tag{72}$$

while the momentum P is, with Eqs. (37) and (38), now defined by

$$P = \lambda_1 + \lambda_2 + \lambda_3 \tag{73}$$

$$\lambda_1 = \frac{1}{3}\, y_2[(v-1)^2 - 1] + \frac{y_3}{2} \tag{74}$$

$$\lambda_2 = \frac{-\Delta T_o}{6(1+m)}\,\{y_2[(v-1)^2(v+1) - 1] + y_3\} \tag{75}$$

$$\lambda_3 = \frac{\Delta T_o^2}{6(1+m)^2}\,\{y_2[(v-1)^2(v^2+1) - 1] + y_3\} \quad . \tag{76}$$

Using Section 4.1, we can develop the flux and momentum equations to the form

$$\mu_1 = \frac{y_{21}}{2} [6 - S(1 - S)^{1/2}] \tag{77}$$

$$\mu_2 = \frac{-y_{21}}{2} \frac{\Delta T_o}{1 + m} \{[(1 - S)(3 - S) - 1](1 - S)^{1/2} + 16\} \tag{78}$$

$$\mu_3 = \frac{y_{21}}{2} \frac{\Delta T_o^2}{(1 + m)^2} \{[(1 - S)(2 - S)^2 - S](1 - S)^{1/2} + 26\} \tag{79}$$

$$\lambda_1 = \frac{y_{21}}{3} \{[(1 - S)^2 - 1](1 - S)^{1/2} + 6\} \tag{80}$$

$$\lambda_2 = \frac{-y_{21}}{6} \frac{\Delta T_o}{1 + m} \{[(1 - S)^2(3 - S) - 1](1 - S)^{1/2} + 16\} \tag{81}$$

$$\lambda_3 = \frac{y_{21}}{6} \frac{\Delta T_o^2}{(1 + m)^2} \{[(1 - S)^2(2 - S)^2 + (1 - S)^2 - 1](1 - S)^{1/2} + 26\} \quad . \tag{82}$$

Because of the dominant effect of the $y_3$ term, the flux and momentum terms vary very little in the Zone II region. We shall, therefore, utilize average values of these quantities in calculating the vertical velocity and trajectory. Integration of the buoyancy equation now yields for the vertical velocity

$$\frac{V}{u_o} = \frac{6}{\mu} \frac{V_1}{u_o} + (x_2 - x_1) \frac{1}{K} \frac{m}{1 + m} \frac{2}{\mu} L \tag{83}$$

where

$$L = \frac{1 - r^{3/2}}{3} + \frac{1 - r^{5/2}}{5} + 3(1 - r) \tag{84}$$

$$\mu = 6 - S(1 - S)^{1/2} \tag{85}$$

$$r = 1 - S \tag{86}$$

in which we have neglected the small contribution of the $\Delta T_o$ terms.

Integration of the trajectory equation yields

$$y = y_1 + \frac{3}{2}\, m \frac{V_1}{u_o} \frac{6}{\lambda} (x - x_1) + \frac{m^2}{1 + m} \frac{1}{K} \frac{3}{\lambda} (x_2 - x_1)^2\, M \tag{87}$$

$$M = \frac{53}{15} S - \frac{2}{15}(1 - r^{5/2}) - \frac{2}{35}(1 - r^{7/2}) - \frac{3}{2}(1 - r^2) \tag{88}$$

$$\lambda = 6 + [(1 - S)^2 - 1](1 - S)^{1/2} \quad . \tag{89}$$

## 5. CALCULATION OF UPPER PORTION OF TRAJECTORY

The calculated results show that the slope of the trajectory at the end of Zone I, $x_1$, is generally near unity and increasing rapidly as it moves toward a vertical position at $x_2$. During this interval the character of the motion has altered from one in which the change of direction is due principally to buoyancy, to one in which it stems primarily from deflection due to wind pressure. The jet velocity drops off more slowly during this interval than during the buoyancy dominated motion. To evaluate the jet velocity at $x_2$, we make use of the constancy of momentum in the direction normal to the jet axis,[11] that is,

$$\rho_1 u_{m1}^2 \delta_1 \sin \alpha_1 = \rho_2 u_{m2}^2 \delta_2 \sin \alpha_2 \tag{90}$$

where $\delta$ is the jet width and $\alpha$ is the angle between the jet velocity and the wind. Since the jet is thoroughly mixed, the densities $\rho_1$ and $\rho_2$ may be taken as equal. The mixing coefficient c is more complex here than in the case of a horizontal jet since the angle between the wind and jet directions is no longer constant. For simplicity, we shall — following Abramovich — assume that the value of c is the same as for a horizontal jet. The value of $\delta_2$ is then easily calculated. A numerical check of Eq. (90) for many tests show that $u_{m2}^2$ is close to 1/2 of $u_{m1}^2$ and, for convenience, we shall use the value 1/2.

As the vertical jet interact with the wind, it is gradually bent over toward a horizontal direction. To obtain this upper trajectory, we employ the method developed by Shandorov for obtaining the path of a jet in a deflecting flow.[12] On the

---

11. Abramovich, G. N. (1963) The Theory of Turbulent Jets, The MIT Press, Cambridge, Mass., Chapter 12, pp 547-548.
12. Abramovich, G. N. (1963) The Theory of Turbulent Jets, The MIT Press, Cambridge, Mass., Chapter 12, pp 541-556.

basis of many experiments, Shandorov gives an empirical equation which, for the case of wind perpendicular to the jet, may be written as

$$\frac{(x_2 - x)}{2\delta} = \left(\frac{y_e - y}{2\delta}\right)^{2.55} \frac{1}{\rho_e} \frac{1}{u_e^2} \tag{91}$$

where $u_e$ is the initial jet velocity, assumed uniform across the jet, $\rho_e$ the jet density, and $y_e$ the initial vertical coordinate, at the position $x_2$. Since the jet is well mixed with air, we may take $\rho_e$ as unity. We shall assume that the velocity profile is linear at $x_2$ and, therefore, calculate the effective value of $u_e$ by

$$u_e^2 = \frac{1}{3} u_{m2}^2 \tag{92}$$

where $u_{m2}^2$ is taken as 0.5.

## 6. DETERMINATION OF LIFT-OFF POINT AND LENGTH OF JET FROM EXPERIMENTAL DATA

In correlating the lift-off point $x_\alpha$ against the experimental data, we shall assume that $x_\alpha$ is proportional to the product of the initial jet velocity $u_o$ and the relative velocity $u_a(m + 1)$ and inversely proportional to the temperature excess $\Delta T_m$ and write

$$x_\alpha \sim \frac{u_o u_a(m + 1)}{g y_o \Delta T_m} \quad . \tag{93}$$

Using Eq. (3) for the temperature excess $\Delta T_m$, and noting that m is large compared to unity, Eq. (93) becomes

$$x_\alpha \sim m^2 K \tag{94}$$

where K is the Froude number for the initial flow. Other powers of the initial and relative velocities may be tried in Eq. (93), leading to different combinations of m and K in Eq. (94). However, the relation given by Eq. (94) appeared to yield the best results.

The results of the correlation are shown in Figure 2 where we have plotted the experimental values of the lift-off point $x_\alpha$ against the parameter $p = m K^{1/2}$.

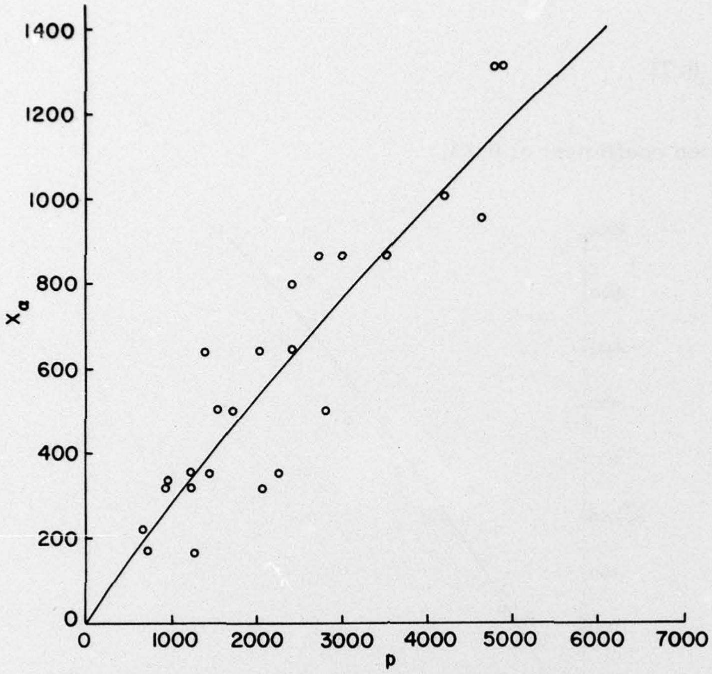


Figure 2. Plot of Experimental Values of Lift-Off Point $x_\alpha$ Against Parameter p; Solid Curve is Power Law Fit to Experimental Points

A fair correlation is obtained, but not as good as that obtained for the coflowing jet. The data has been fitted with a power law curve with the result,

$$x_\alpha = 0.66\, p^{0.88} \tag{95}$$

and a correlation coefficient of 0.79.

Although the jet length $x_2$ may be calculated from the model, as shown in reference 8, it is desirable to be able to obtain $x_2$ from the parameters of the experiment. Since the jet is buoyant, it should depend upon the same parameter used in determining the lift-off point. In addition, in view of the initial heating of the jet, $x_2$ should drop off inversely to the inlet jet temperature $T_o$. However, the use of $T_o$ in the correlation did not result in any visible improvement of the results. We have, therefore — for convenience — utilized the same parameter p for jet length as previously used for lift-off point. The results of the correlation are shown in Figure 3 where $x_2$ is plotted against p. The amount of scatter is about the same as that obtained for $x_\alpha$. A power law curve has been fitted to the data yielding

$$x_2 = 4.02\, p^{0.71} \tag{96}$$

with a correlation coefficient of 0.83.

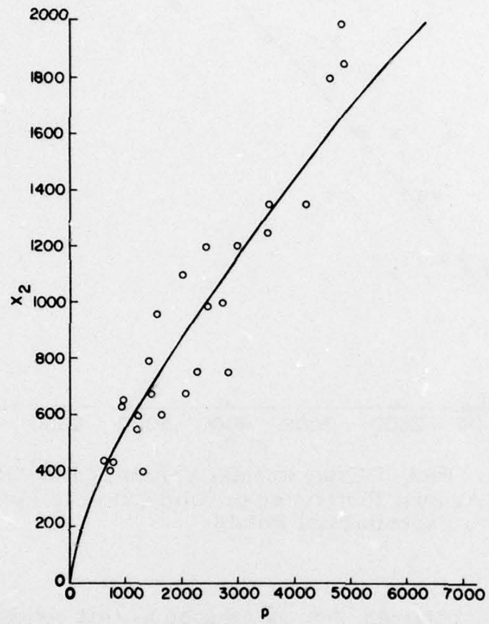


Figure 3. Plot of Experimental Values of Jet Length $x_2$ Against Parameter p; Solid Curve is Power Law Fit to Experimental Points

## 7. RESULTS AND DISCUSSION

The calculated trajectories are shown in Figures 4-9 along with the corresponding experimental curves. These results cover most of the range of windspeeds, initial jet velocities, and initial jet temperatures encountered in the tests. The calculated results are in fair agreement with the experimental curves, but the lower portion of the calculated trajectory generally tends to be somewhat higher than the corresponding experimental result. The lower buoyancy observed experimentally may be due to the fact that when the jets merge, the assumed equivalent planar jet contains regions of cooler air between the jets which help lower the total buoyant force of the jet. In addition, when the jet detaches from the ground some jet air may become entrained with the ambient air going under the jet, resulting in

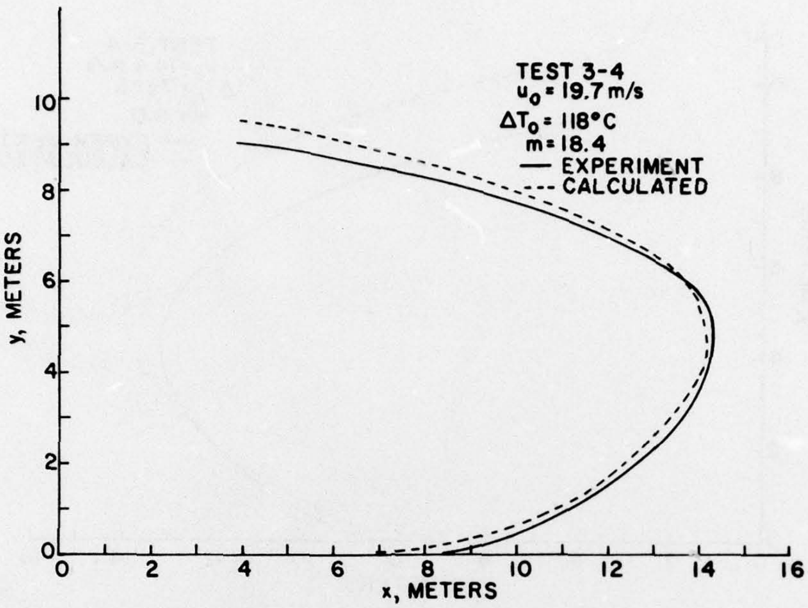


Figure 4. Comparison of Calculated Trajectories, for Several Tests, with Corresponding Experimental Curves, Test 3-4

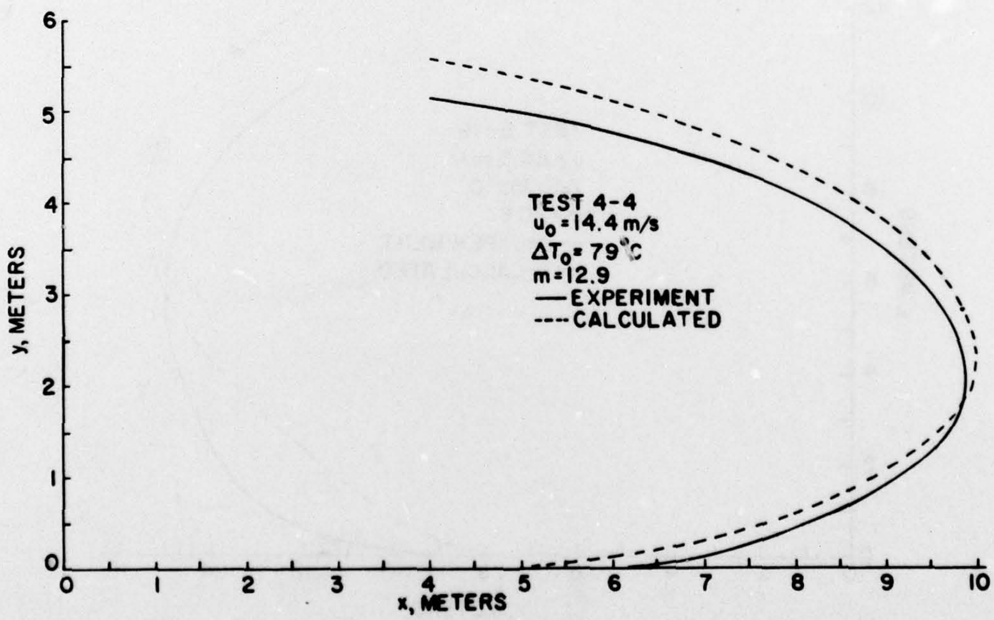


Figure 5. Comparison of Calculated Trajectories, for Several Tests, with Corresponding Experimental Curves, Test 4-4

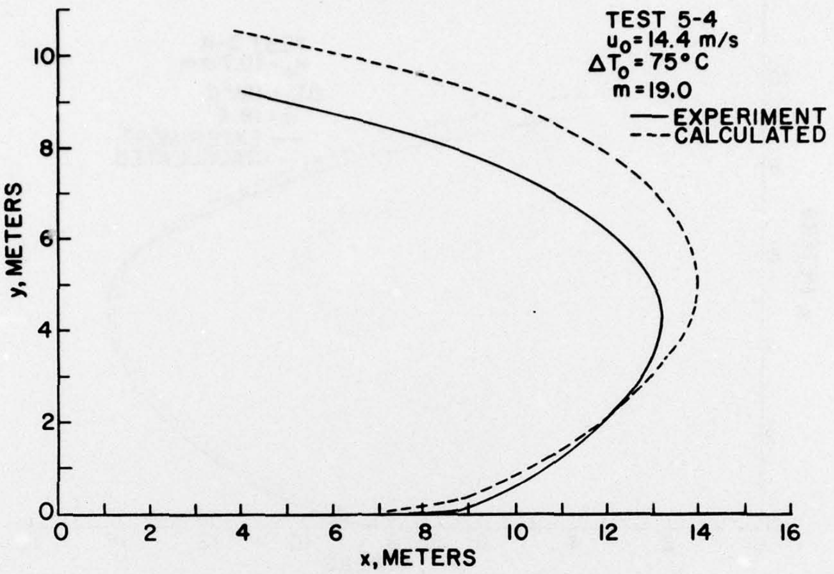


Figure 6. Comparison of Calculated Trajectories, for Several Tests, with Corresponding Experimental Curves, Test 5-4

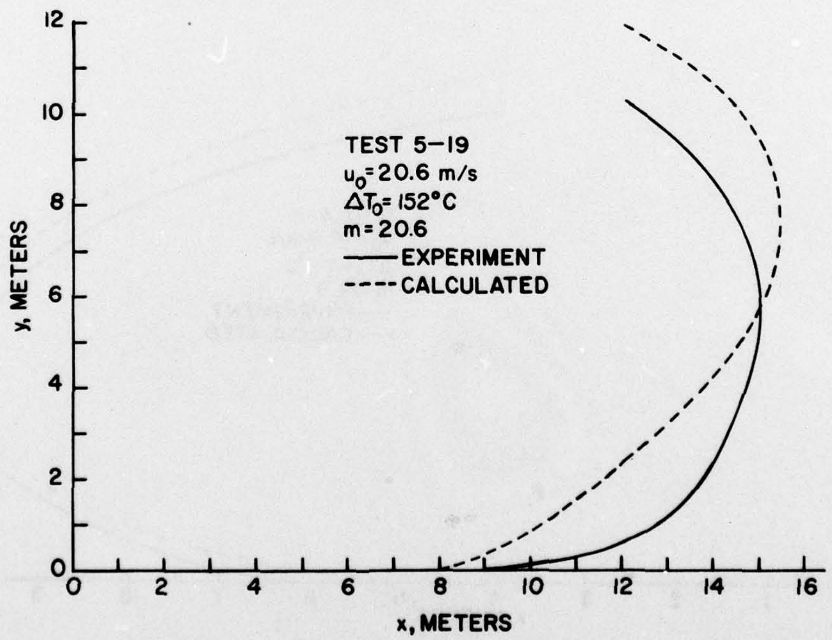


Figure 7. Comparison of Calculated Trajectories, for Several Tests, with Corresponding Experimental Curves, Test 5-19

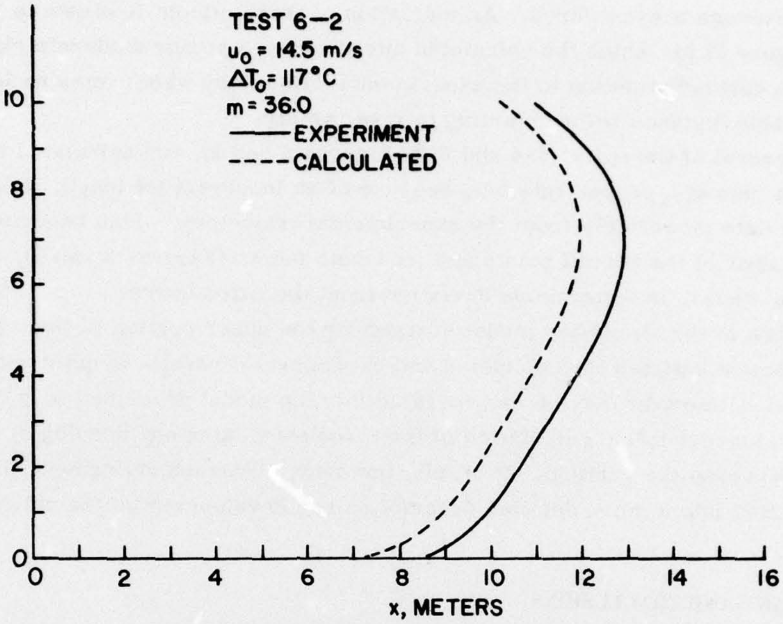


Figure 8. Comparison of Calculated Trajectories, for Several Tests, with Corresponding Experimental Curves, Test 6-2

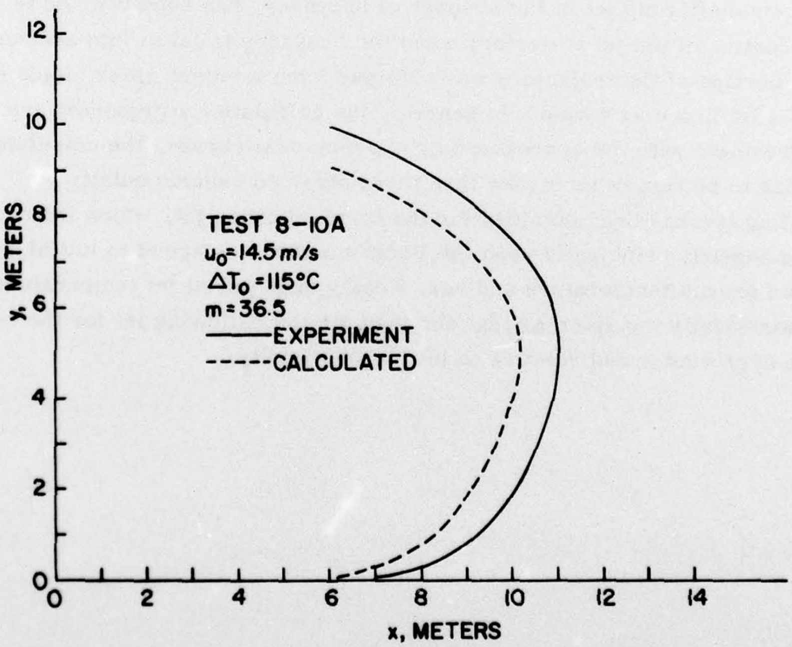


Figure 9. Comparison of Calculated Trajectories, for Several Tests, with Corresponding Experimental Curves, Test 8-10A

lower average buoyant force. An indication of these effects is shown in Test 5-19 (Figure 7) for which the calculated curve shows a steady moderate rise after lift-off in contradistinction to the experimental trajectory which remains low a considerable distance before starting to rise rapidly.

In several of the tests, 5-4 and 6-2 (Figures 6 and 8), the calculated curves appear to rise at a proper rate but, because of an incorrect jet length or lift-off point, deviate moderately from the experimental trajectory. This behavior is due to the scatter of the lift-off points and jet length points (Figures 2 and 3), resulting, in several cases, in appreciable deviation from the fitted curves.

In view of the simplified model utilized for the upper portion of the trajectory, the agreement between the calculated and experimental results is quite reasonable. Additional refinement may be incorporated into the model described in Section 5, that is, a more detailed calculation of the turbulent mixing and bending of the curve as it approaches the vertical. It is felt, however, that such refinement should be incorporated into a more detailed description and development of the entire model.

## 8. SUMMARY AND CONCLUSIONS

A model, previously developed for obtaining the dynamic properties of a heated turbulent counterflowing jet in the absence of buoyancy, has been utilized to obtain the lower portion of the jet trajectory when the buoyancy is taken into account. The upper portion of the trajectory was obtained from a model which yields the deflection of a jet in a cross wind. In general, the calculated trajectories are in fair to good agreement with the corresponding experimental curves, the calculated results tending to be somewhat higher than those obtained experimentally.

A scaling law has been obtained for the counterflowing jet, which indicates that the scaling depends principally upon the Froude number referred to initial jet velocity and excess temperature and very weakly upon initial jet temperature. This result is essentially the same as that obtained for the coflowing jet for the case of small values of wind speed relative to initial jet velocity.

## References


1. Abramovich, G. N. (1963) The Theory of Turbulent Jets, The MIT Press, Cambridge, Mass., Chapters 4 and 9.
2. Abramovich, G. N. (1963) The Theory of Turbulent Jets, The MIT Press, Cambridge, Mass., Chapter 12, pp 580-585.
3. Klein, M. M., and Kunkel, B. A. (1975) Interaction of a Buoyant Turbulent Planar Jet With a Coflowing Wind, AFCRL-TR-75-0368.
4. Klein, M. M., and Kunkel, B. A. (1975) Interaction of a Buoyant Turbulent Round Jet With a Coflowing Wind, AFCRL-TR-75-0581.
5. Klein, M. M. (1977) A Method for Determining the Point of Lift-Off and Modified Trajectory of a Ground-Based Heated Turbulent Planar Jet in a Coflowing Wind, AFGL-TR-77-0033.
6. Abramovich, G. N. (1963) The Theory of Turbulent Jets, The MIT Press, Cambridge, Mass., Chapter 4.
7. Sekundov, A. N. (1969) The Propagation of a Turbulent Jet in an Opposing Stream, in Turbulent Jets of Air, Plasma and Real Gas, Consultants Bureau, New York.
8. Klein, M. M. (1977) Interaction of a Turbulent Planar Heated Jet With a Counterflowing Wind, AFGL-TR-77-0214.
9. Kunkel, B. A. (1975) Heat and Thrust Requirements of a Thermal Fog Dispersal System, AFCRL-TR-75-0472.
10. Abramovich, G. N. (1963) The Theory of Turbulent Jets, The MIT Press, Cambridge, Mass., Chapter 1, pp 32-36.
11. Abramovich, G. N. (1963) The Theory of Turbulent Jets, The MIT Press, Cambridge, Mass., Chapter 12, pp 547-548.
12. Abramovich, G. N. (1963) The Theory of Turbulent Jets, The MIT Press, Cambridge, Mass., Chapter 12, pp 541-556.

# List of Symbols

| | |
|---|---|
| b | distance from outside wall to jet axis |
| c | jet thickness coefficient |
| $H$ | *end of initial section* |
| K | Froude number |
| m | wind speed parameter = $u_o/u_a$ |
| p | jet parameter = $m\,K^{1/2}$ |
| T | jet temperature |
| $T_a$ | ambient temperature |
| $T_m$ | temperature on axis |
| $\Delta T$ | temperature excess over ambient $(T - T_a)$ |
| u | jet velocity |
| $u_m$ | velocity on axis |
| V | vertical velocity |
| x | horizontal position along jet |
| $x_H$ | end of initial section |
| $x_1$ | end of Zone I |
| $x_2$ | end of Zone II |

| | |
|---|---|
| $x_\alpha$ | lift-off position |
| $y$ | vertical position |
| $y_o$ | jet half-width |
| $y_2$ | zero velocity surface in main section |
| $y_3$ | surface separating perturbed and unperturbed flows |
| $\alpha$ | angle between jet and wind |
| $\rho$ | gas density |
| $\delta$ | jet width |

Subscripts

| | |
|---|---|
| a | ambient |
| c | region above $y_3$ surface |
| m | on jet axis |
| o | initial jet position |
| $\alpha$ | lift-off position |
| e | *initial position* |